Paper No. 409. (quote when citing this article)
Eleventh World Conference on Earthquake Engineering
ISBN: 0 08 042822 3

SEISMIC PERFORMANCE OF HALF PRECAST BEAMS WITH LAPPING BAR SPLICES UNDER SHEAR FORCES

H. IMAI
Institute of Engineering Mechanics University of Tsukuba
Tennoudai 1-1-1, Tsukuba City, Ibaraki 305, Japan

A. HATAHIRA
Institute of Engineering Mechanics University of Tsukuba
Tennoudai 1-1-1, Tsukuba City, Ibaraki 305, Japan

K. SAITO
Central Research Institute of Electric Power Industry
Abiko 1648, Abiko City, Chiba 270-11, Japan

ABSTRACT

An experimental investigation on the seismic performance of half precast beams with lapping bar splices was conducted. The specimens were subjected to continuous cyclic loads producing anti-symmetrical bending moments. To investigate the change in the failure mode of the beam from shear to flexural failure , two parameters were varied : shear-flexural capacity ratio and the amount of lateral reinforcement. Test results indicated that for specimens having a shear-flexural capacity ratio greater than 1.2 flexural failure occurred , whereas shear failure (including shear failure accompanied by slippage at the horizontal concrete joint) and bond splitting occurred when the bond capacity ratio/shear-flexural ratio=1.6/1.2 was the boundary condition.

KEYWORDS

precast beam, lapped joint, horizontal concrete joint, shear, bond

INTRODUCTION

A relatively new economical method of precast connection known as the main bar post insertion method is utilized in this study. This method, which provides both seismic resistance and construction efficiency, focuses on two remarkable points : the main bars are jointed at the center of the members where seismic forces are small, and the precast elements are simple such as beams and columns. In this method, a simple and economical bar joint system is proposed wherein in the casting of the precast members, instead of main bars, metallic corrugated sheaths and lapping bars are embedded at the position of main bars together with the lateral reinforcement. At the construction site, the main bars are then inserted into the sheaths and after which high-strength mortar is grouted, effectively fixing the main bars in the sheaths.

This study aims to further investigate the seismic behavior of precast beams using the proposed connection technique. Specifically, this study aims to examine the effect of varying the shear-flexural capacity ratio and the amount of lateral reinforcement on the transition of the beam failure mode from shear to flexural failure.

OUTLINE OF SPECIMENS

A total of 15 specimens were tested. A layout of a typical specimen is shown in Fig. 1. The specimens are 2/3 the size of rectangular composite beams at the lower floor of middle or high-rise buildings in Japan. Each specimen is 340 mm wide, 500mm high, and 2000 mm long. As shown in Fig. 1(b), the lower part of the cross-section having a height of 350 mm is precast and the upper portion having a height of 150mm is cast-in-situ. The horizontal concrete joint surface of the precast element was roughened using a wire brush about one hour after concrete was compacted.

Table 1 summarizes the details of the specimens. The amount of lateral reinforcement was varied in all specimens. The

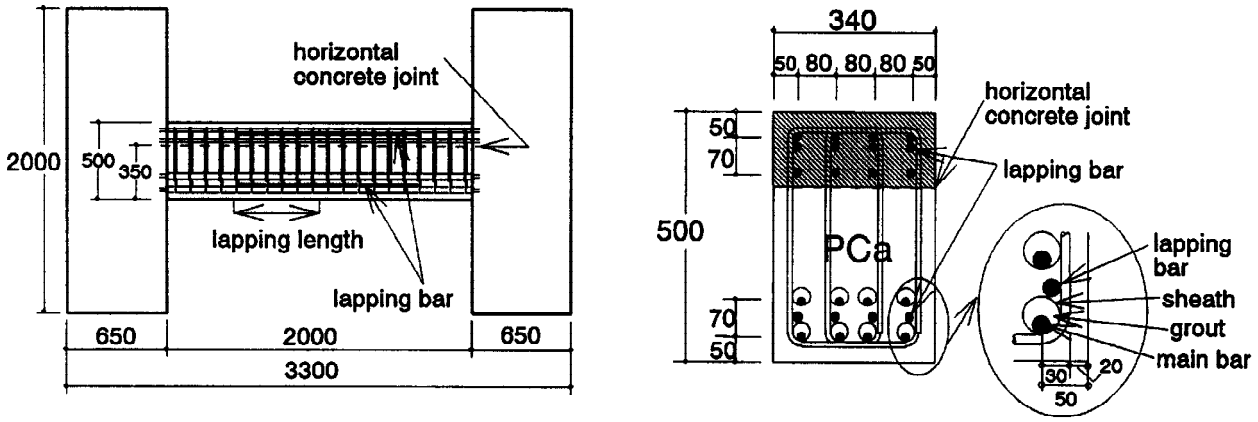

(a) Outline (b) Cross Section of Precast Beam

Fig. 1 Outline of Specimen

Table 1 Properties of Specimens

Specimen	Main Bar		Stirrup				Shear-Flexural Capacity Ratio $Q_{su.A}/Q_{mu}$
	Size	Specified Yield Strength(kgf/cm^2)	Size	Pitch (p_w %)	Specified Yield Strength (kgf/cm^2)	Reinforcing Amount $p_w \sigma_{wy}$(kgf/cm^2)	
B21	8-D22	7000	4-D10	100mm(0.84)	3000	30.0	0.75
B22				150mm(0.56)		19.3	0.57
B23		4000		90mm(0.93)		32.1	1.45
B24				110mm(0.73)		26.2	1.26
B25				150mm(0.56)		19.3	1.02
B26	8-D19			110mm(0.76)		26.2	1.70
B27				140mm(0.60)		20.7	1.44
B31	8-D25	7000	4-D10	70mm(1.20)	3000	36.0	0.85
B32				80mm(1.05)	3500	36.7	0.81
B33				185mm(0.45)	8000	36.0	0.81
B34			4-H7	170mm(0.28)	13000	36.4	0.59
B35			4-D10	140mm(0.60)	3000	18.0	0.57
B36					3500	21.0	0.57
B37					8000	48.0	0.90
B38			4-H7	80mm(0.59)	13000	76.7	0.91

p_w: Lateral Reinforcement Ratio

$$\text{Shear - Flexural Capacity Ratio} = \frac{\text{Shear Strength } Q_{su.A}}{\text{Flexural Strength } Q_{mu}}$$

Shear Strength: Method A of the shear strength equation of AIJ (1)
Flexural Strength: Ultimate Flexural Strength (2)

$$Q_{su.A} = b j_t p_w \sigma_{wy} \cot\phi + \tan\theta(1-\beta) b D \nu \sigma_B / 2 \quad (1)$$

where $\beta = \left\{\left(1+\cot^2\phi\right) p_w \sigma_{wy}\right\} / \left(\nu \sigma_B\right)$

$$Q_{mu} = 0.9 A_t \sigma_{wy} d / L \quad (2)$$

where A_t= total area of the main bars
σ_{wy}= specified yield strength
d= depth of the beam
L= beam length

design shear-flexural capacity ratio, which was regulated by varying the diameter and the strength of the main bar and the pitch or the yield strength of stirrups for each of the specimen, was calculated using a specified concrete strength of 300kgf/cm^2 and the specified yielding strength for the main bars and assuming conventional monolithic reinforced

concrete beams.

The main bars were abutted at midspan and had lap splices located at the middle portion of the beams. The lapped length used was 30d (d: the main bar diameter) in B21 to B27 and 26.4d in B31 to B38. Both the top and bottom main bars were double-layered wherein only the outer layers are spliced with lapping bars having equal diameter and strength as the main bar as shown in Fig.1(b). No lapping bar was placed in the inner layers of main bars.

The specimens were cast in the following manner. First, the sheaths were placed at the position of each bottom main bar and the precast element containing the stirrups and the bottom lapping bars was cast. Next, the bottom main bars are inserted into the sheaths and the top main bars together with the lapping bars were arranged. The concrete was then cast on the upper beam section together with the support columns at both ends of the beam. After concrete hardening, the grout was injected into the sheaths using previously embedded pipes. All main bars were then anchored in the support columns.

The specified strengths of concrete and grout were 300 kgf/cm^2 and 600 kgf/cm^2, respectively. Material test results show that the strength of the rebars, concrete and grout were relatively close with their respective specified values.

LOADING SYSTEM AND INSTRUMENTATION

A schematic drawing of the loading set-up is shown in Fig. 2. Each specimen was subjected to varying shear forces applied continuously in a cyclic manner producing anti-symmetrical bending moments. Both columns were restrained from horizontal movement by high-strength anchor bars and oil jacks placed at the upper and lower ends of the beam. Shear span ratio is equal to 2.0. The application of shear forces was controlled by the following loading history: each specimen was subjected to one cycle of loading at a drift angle R equal to 1/800, two cycles of loading at R equal to 1/400, 1/200, 1/100, 1/50, and again one cycle at R equal to 1/25. The lateral drift angle R is defined as the total relative displacement of the columns divided by the length of the beam.

Two sets of devices were used to measure the deformations of the specimens. The total lateral displacement in the front and back sides of the beam was directly measured by linear variable displacement transducers (LVDTs) positioned at the midheight of the specimen as shown in Fig. 3. To measure partial deformations, each specimen was divided into eleven regions and clip gauges were attached to measure the shear and flexural deformations of each region. Also, the slippage at the horizontal concrete joint and the strains of the main bars and stirrups were measured. The development of cracks in each specimen was carefully observed and recorded by marking the cracks at the peaks of each load cycle.

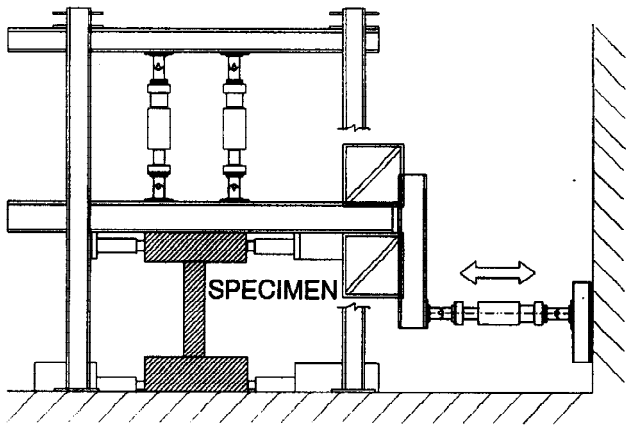

Fig. 2 Loading Apparatus

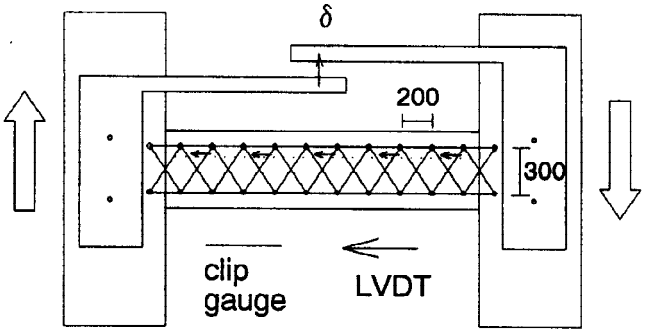

Fig. 3 Instrumentation

TEST RESULTS AND DISCUSSION

Load-displacement relationship and crack pattern

Typical load-displacement hysteresis loops for specimens failing in different modes are shown in Fig. 4. Schematic illustrations of the crack patterns on the front side of these specimens are shown in Fig. 5.

For shear failure type specimen B22, failure in shear accompanied by slippage at the horizontal concrete joint occurred

before flexural yielding of the main bars. After the ultimate strength was reached, the load-displacement curve started to exhibit an inverse S-shaped behavior. Cracks opened at the ends and propagated towards the central surface of the beam and by the end of the test, these cracks caused spalling of the concrete.

For shear failure type specimen B25 having a higher shear-flexural capacity ratio than B22, slippage at the horizontal concrete joint occurred after flexural yielding of the main bars. After the second excursion of R=1/50, due to the onset of slippage at the concrete joint, the hysteresis loop showed a sudden degradation of stiffness and load-carrying capacity. Small crack damages are concentrated at the beam ends and along the horizontal concrete joint.

For flexural failure type specimen B26, the load-displacement relation shows good hysteretic performance and ultimate strength is reached at R=1/25. Flexural cracks opened at the beam ends and were excessive at the final stage. No slippage at the horizontal concrete joint took place.

B32, which had normal strength stirrups at narrow spacing, failed in shear. At R=1/50, shear cracks spread uniformly at the central part of the beam. At the same time, the stirrups yielded and the specimen failed in shear. It can be considered that shear failure occurred because the stirrups at narrow spacing could confine the concrete in spite of the stirrups yielding.

B34, which had high strength stirrups wide spacing, failed in bond. At R=1/100, bond cracks occurred around the splice of the second layer. At the final stage, bond failure was very much evident around the sheath of the second layer. The stirrups could not confine the concrete effectively because of the wide spacing.

No difference of hysteretic performance was noticed whether it was shear failure or bond failure.

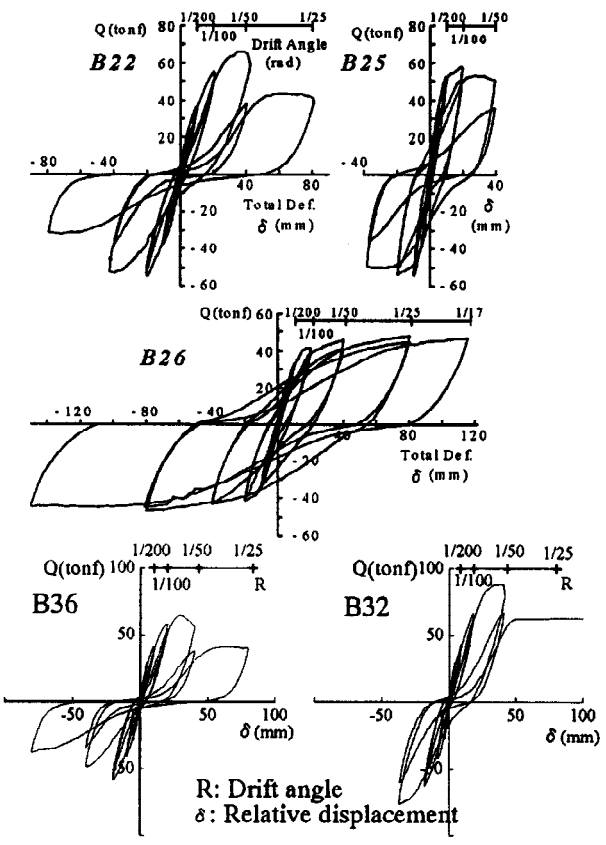

Bond Failure Shear Failure

Fig. 4 Load-Displacement Relations

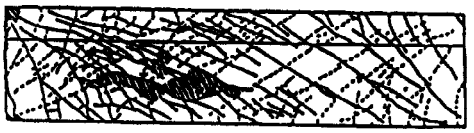

(a) B22 Shear Failure (Slippage at the concrete joint)

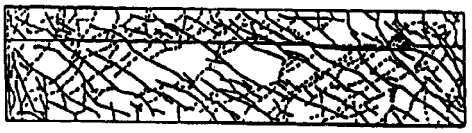

(b) B25 Shear Failure (Slippage occurring after flexural yielding)

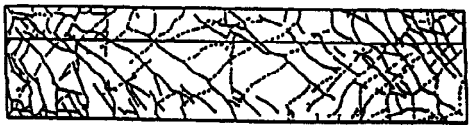

(c) B26 Flexural Failure

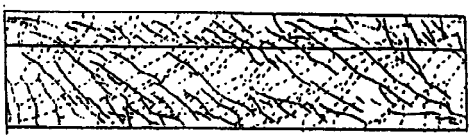

(d) B32 Shear Failure by Tension

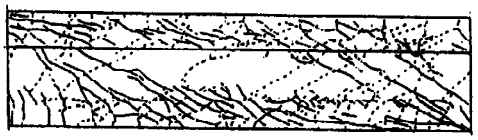

(e) B34 Bond Failure

Fig. 5 Crack Patterns

Maximum loads

The calculated and experimental maximum loads are listed in Table 2. The maximum loads were calculated assuming monolithic beams and using the material properties obtained from actual testing. The types of failure attained by the specimens at the final stage are classified as shear failure accompanied by slippage at the horizontal concrete joint and

flexural failure.

Figure 6 shows a graph of the ratio of the maximum load sustained by the specimen Qmax to the calculated flexural capacity Qmu versus the shear-flexural capacity ratio. Here, the types of failure exhibited by the specimens are clearly identified. This graph also incorporates results of previous experiments on a similar study. In a shear failure type, slippage at the horizontal concrete joint occurring before yielding of the main bar is observed. However, slippage can also be observed as occurring some time after the main bars have yielded. On the other hand, for a flexural failure type, the maximum load attained exceeded the predicted flexural capacity for the specimens by about 10-30% which is a similar results in the flexural capacities of monolithic beams. However, for specimens failing in both shear and bond, the maximum load attained are relatively close to the shear capacity predicted by Method A of the shear strength equation of AIJ (1).

Table 2 Experimental and Calculated Maximum Loads

Specimen	Experimental Values		Calculated Values		Experimental /Calculated		Shear-Flexural Cap. Ratio	Failure Type
	Drift Angle R	Q_{max} (tonf)	Q_{mu} (tonf)	$Q_{su.A}$ (tonf)	$\frac{Q_{max}}{Q_{mu}}$	$\frac{Q_{max}}{Q_{su.A}}$	$\frac{Q_{su.A}}{Q_{mu}}$	
B21	1/55	72.5	74.7	74.8	0.97	0.97	2.17	SL
B22	1/54	66.4		56.0	0.89	1.19	1.00	SL
B23	1/25	59.7		80.4	1.13	0.74	0.75	F→FC
B24	1/25	60.6	52.9	70.6	1.15	0.86	1.52	F→FC
B25	1/50	58.0		57.1	1.10	1.02	1.34	F→SL
B26	1/25	47.9	39.1	70.4	1.23	0.68	1.08	F→FC
B27	1/25	47.9		59.6	1.23	0.80	1.80	F→FC
B31	1/50	83.1		88.3		0.94	0.85	St
B32	1/52	87.9		84.4		1.04	0.81	St
B33	1/54	74.3		84.2		0.88	0.81	St→BO
B34	1/61	65.9		60.6		1.09	0.58	Sc→BO
B35	1/61	65.8	103.7	59.4	0.80	1.11	0.57	St→BO
B36	1/68	65.2		59.5		1.10	0.57	St→BO
B37	1/51	75.3		93.7		0.80	0.90	St→BO
B38	1/50	84.5		94.2		0.90	0.91	Sc→BO

F: Flexural Yielding FC: Flexural Failure SL: Shear Failure and Slippage
Sc: Shear Failure by Compression St: Shear Failure by Tension BO: Bond Splitting Failure
Q_{mu}: Ultimate Flexural Strength (2)
$Q_{su.A}$: Ultimate Shear Strength by AIJ (Method A) (1)

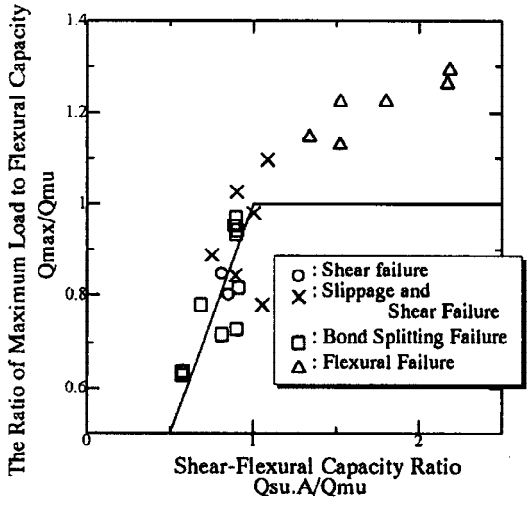

Fig. 6 Shear-Flexural Capacity Ratio and Maximum Strength Relations

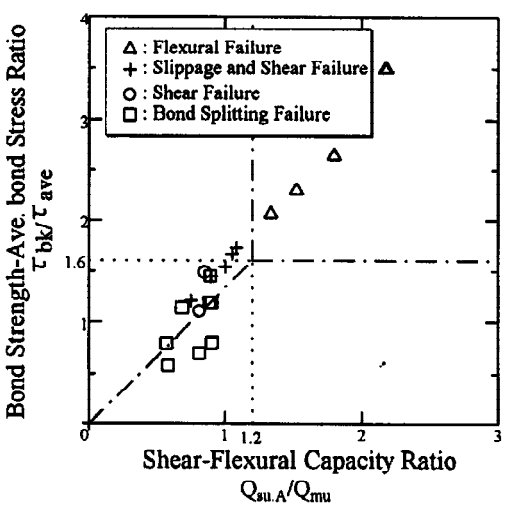

Fig. 7 Shear-Flexural Capacity Ratio and Bond Strength-Ave. Bond Stress Ratio

Bond strength to average bond stress ratio

Figure 7 shows the relation between the shear-flexural capacity ratio and the bond strength to average bond stress ratio. The average bond stress τ_{ave} was obtained assuming the bars at both ends of the beam are yielding in tension and compression and that bond stress is zero at a section 1D (D: beam depth) of the tension side of the member due to inclined cracks or yield hinge. The bond strength τ_{bk} is calculated from the bond splitting strength equation proposed by Kaku-Zhang as is shown in the following equation:

$$\tau_{bk} = \left[0.08 + 0.12b_i + k_n\left(q \cdot b_i + 18.0p_w / (Nd_b)\right)\right] \cdot \sigma_B^{0.6} \quad (3)$$

Here, if $\sigma_{wy} \le 115\sigma_B^{0.6}$, then $\sigma_{wy} = 115\sigma_B$

$b_i = b/(N \cdot d_b) - 1$, $k_n = 1.0 + 0.85(n-2)/N$, $q = (2.5 + 875p_w)/(l_b/d_b + 7000p_w)$

N: the number of main bars

n: the number of stirrups per unit

l_b: lapped length

d_b: the diameter of the main bar or the sheath

The different modes of failure exhibited by the specimens are indicated in the graph. The following results can be inferred from the graph:

Flexural failure: a shear-flexural capacity ratio above 1.2 and bond strength-average bond stress ratio over 1.6.

Shear and Slippage failure: a shear-flexural capacity ratio below 1.2 and $\left(\frac{\tau_{bk}}{\tau_{ave}}\right)\Big/\left(\frac{Q_{su.A}}{Q_{mu}}\right) \ge \frac{1.6}{1.2}$

Bond Failure: a bond strength-average bond stress ratio below 1.6 and $\left(\frac{\tau_{bk}}{\tau_{ave}}\right)\Big/\left(\frac{Q_{su.A}}{Q_{mu}}\right) \le \frac{1.6}{1.2}$

A distinction on the boundary, however, between shear and bond splitting failures cannot be recognized precisely.

Flexural and Shear Components of total deformation

The relationship between shear-flexural capacity ratio and the flexural component of the total lateral deformation at every peak of the positive loading cycles is shown in Fig. 8. The flexural deformation are obtained from the curvatures measured by the clip gauges attached to each of the eleven equally divided regions of the beam. Up to lateral drift angle of R=1/200, the flexural deformation contributed to about 80% of the total deformation for all specimens while the remaining deformation was due to shear. Despite a continuous increase in the total deformation, the shear and flexural deformation distribution remains constant for all specimens having a shear-flexural capacity ratio above 1.2. However, for specimens having a shear-flexural capacity ratio below 1.2, the flexural deformation component ratio decreases with an increase in total deformation with the decrease becoming more evident as the shear-flexural capacity ratio becomes smaller.

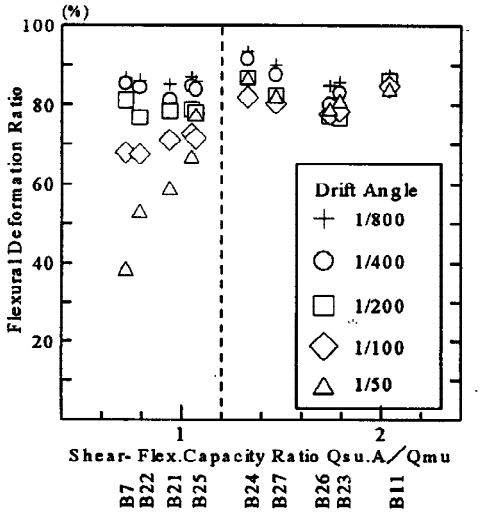

Fig. 8 Shear-Flexural Capacity Ratio and Flexural Deformation Ratio

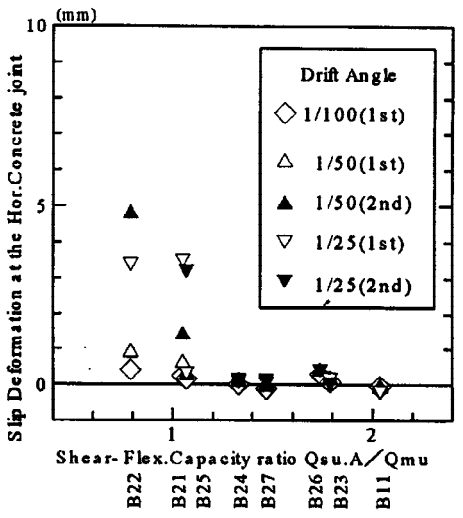

Fig. 9 Shear-Flexural Capacity Ratio and Slippage at the Concrete Joint

Slip deformation at the horizontal concrete joint

The relationship between shear-flexural capacity ratio and slip deformation of the horizontal concrete joint at the middle part of the specimen at every peak of the loading cycles is shown in Fig. 9. Both first and second excursions of R=1/50 and R=1/25 are shown in the graph.

For specimens with a shear-flexural capacity ratio above 1.2, no slippage occurred at the horizontal concrete joint. All these specimens not experiencing any degree of slipping at the concrete joint failed in flexure. For a shear-flexural capacity ratio below 1.2, failure in shear accompanied by slippage at the horizontal concrete joint which started after the excursion of R=1/50 can be predicted at the final stage.

For specimen B25, although no slippage occurred at the first excursion (▽) of R=1/25, the second excursion(▼) displayed large slipping at the horizontal concrete joint. For this specimen slippage at the concrete joint took place after a significant increase in the total deformation which is due to the yielding of the main bars.

For specimen B22 with the least value of shear-flexural capacity ratio, a comparison of the slippage after each first (△) and second(▲) excursion of R=1/50 showed that large slippage at the concrete joint occurs regardless of whether or not there is a remarkable increase in the total deformation which is assumed to influence the amount of slippage. Once slippage initiates, the concrete bond between the two contact surfaces is immediately lost. The severity of the slippage towards the final stage can be attributed to the yielding of the stirrups near the horizontal concrete joint.

Strain of the Lateral Reinforcement at the Horizontal Concrete Joint

Figure 10 shows the relationship between the shear-flexural capacity ratio and the strain of the lateral reinforcement at the horizontal concrete joint at the peak of each load cycle. The strains were measured by strain gauges placed on the reinforcement about 10mm below the concrete joint. Strains are observed to be largest at this portion as reported in the study done by Ozawa (1992).
For a shear- flexural capacity ratio above 1.2, the strain is within the elastic region and no slippage is observed. However for a shear-flexural capacity ratio below 1.2 , after the excursion of the load cycle R=1/50 , tension yielding of the lateral reinforcement occurred at the middle portion of the beam. Regardless of the shear-flexural capacity ratio of the specimens, the lateral reinforcement at the beam ends remain within the elastic region up to the final stage. This can be attributed to the presence of rigid columns providing adequate restraint at that portion of the beam.

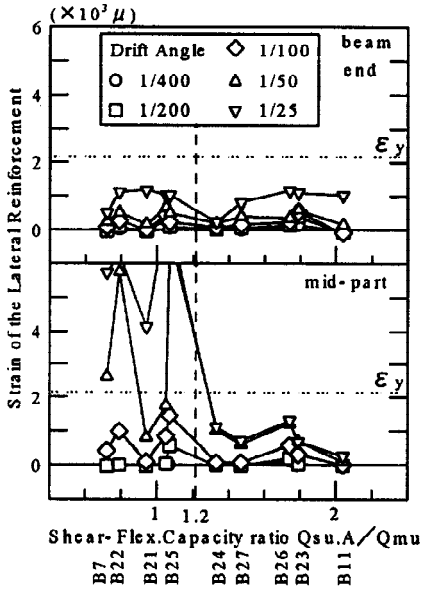

Fig. 10 Shear-Flexural Capacity Ratio and Strain of the Lateral Reinforcement at the Horizontal Concrete Joint

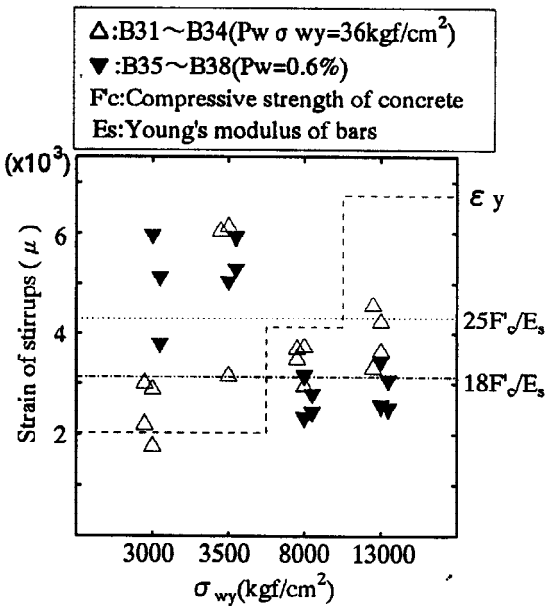

Fig. 11 The Effect of High Strength Stirrups

The Effect of High Strength Stirrups

With reinforcing amount of stirrups constant, the strain of the closely spaced normal strength stirrups of B31 and B32 were greater than the yield strain at the center of the beam while that of the widely spaced high strength stirrups of B33 and B34 were less than the yield strain as is shown in Fig. 11. In this case, even if high strength stirrups were used,

their full capacity could be not attained. On the other hand, with shear reinforcement ratio constant, the strains of the normal strength stirrups of B35 and B36 were larger than the value corresponding to 25Fc' [the critical condition of the shear strength equation (method A)] of AIJ. The strains of the high strength stirrups of B37 and B38 were less than the value corresponding to 25Fc' (Fc': concrete strength), and 18Fc' can be considered more suitable.

CONCLUSION

Based upon the results of the experimental investigation of half-precast beams in the main bar post insertion system, the following conclusions were obtained:

1) Failure attained by the beams are classified into three types: flexural failure, shear failure accompanied by slippage at the horizontal concrete joint, and bond splitting failure.
2) The flexural capacity of the specimens which failed in flexure exceeded the calculated flexural capacity for monolithic beams by about 10-30% which is a similar result in the flexural capacities of monolithic beams.
3) The shear capacity of the specimens which failed in shear and slippage at the horizontal concrete joint, can be predicted using commonly used shear strength equations for monolithic beams.
4) For a shear-flexural capacity ratio near a value of 1.2, changes can be observed on the distribution of the total deformation, slippage at the horizontal concrete joint, and the strains in the lateral reinforcement at the concrete joint. The nature of these changes provided the basis of classification of the end failure mode of the beam specimens.
5) The failure modes can be distinguished accordingly as shown below.

Flexural failure: a shear-flexural capacity ratio above 1.2 and bond strength-average bond stress ratio over 1.6.

Shear and Slippage failure: a shear-flexural capacity ratio below 1.2 and $\left(\frac{\tau_{bk}}{\tau_{ave}}\right) \Big/ \left(\frac{Q_{su.A}}{Q_{mu}}\right) \geq \frac{1.6}{1.2}$

Bond Failure: a bond strength-average bond stress ratio below 1.6 and $\left(\frac{\tau_{bk}}{\tau_{ave}}\right) \Big/ \left(\frac{Q_{su.A}}{Q_{mu}}\right) \leq \frac{1.6}{1.2}$

6) By the knowledge of the shear-flexural capacity ratio and the bond strength-average bond stress ratio of the beam alone, a distinction on the boundary between shear and bond failures cannot be precisely done.
7) Normal strength lateral reinforcements (σ_{wy}= 3000 kgf/cm^2 and 3500 kgf/cm^2) yielded, while the high strength lateral reinforcements (σ_{wy}= 8000 kgf/cm^2 and 13000 kgf/cm^2) did not yield whose stress corresponded to about 18 times the strength of concrete.

REFERENCES

Castro J. J., Imai H and Yamaguchi T. (1994). Seismic Performance of Precast Concrete Beam-Column Joints. *Journal of Structural and Construction Engineering, Transactions of Architectural Institute of Japan,* **455**, 113-126.

Yanez, R., Castro, J. J., Yamaguchi, T., Imai, H. (1995). An Experimental Study on Joint Strength of Spliced Bars using Spiral Sheaths for Precast Concrete Structures. *Journal of Structural and Construction Engineering of AIJ,* **469**, 91-104.

AIJ (1990). *Design Guideline for Earthquake Resistant Reinforced Concrete Buildings based on Ultimate Strength Concept*

Saito, K. , Yamaguchi, T. and Imai, H. (1994) Seismic Performance of Precast Concrete Beams with Lapping Bar Splices under Shear Forces (in Japanese). *Proceedings of the Japan Concrete Institute*, **16**, No.2, 787-792.

Ozawa, K., Makiya, E., Ogawa, S., Nishioka, K.(1992) Shear Resistance for Connection of Precast Concrete Units-part 1. Dowel Action under Monotonous Loading (in Japanese), *Annual Meeting of AIJ (Structure II)*, **21290**, 753-754.

Kaku, T., Zhang, J., Iizuka, S., and Yamada, M. (1992). The Proposal of Equation for Bond Splitting Strength of RC Members including High Strength Concrete Level (in Japanese). *Concrete Research and Technology,* **3**, No. 1, 97-108